Sensitivity of Landsat NDVI to subpixel vegetation and topographic components in glacier forefields: assessment from high-resolution multispectral UAV imagery

Arthur Bayle, Erwan Roussel, Bradley Z Carlson, Franck Vautier, Claire Brossard, Elise Fovet, Géraud De Bouchard D'Aubeterre, Dov Corenblit

Sensitivity of Landsat NDVI to subpixel vegetation and topographic components in glacier forefields: assessment from high-resolution multispectral UAV imagery

Arthur Bayle[a,*] **Erwan Roussel**[b] **Bradley Z. Carlson**[c] **Franck Vautier**[d] **Claire Brossard**[d] **Elise Fovet**[d] **Géraud de Bouchard d'Aubeterre**[b] **and Dov Corenblit**[b]

[a]University of Grenoble Alpes, University of Savoie Mont Blanc, CNRS, LECA, Grenoble, France

[b]Université Clermont Auvergne, CNRS, GEOLAB, Clermont-Ferrand, France

[c]Observatoire du Mont-Blanc, Centre de Recherches sur les Écosystèmes d'Altitude, Chamonix, France

[d]Université Clermont Auvergne, CNRS, Maison des Sciences de l'Homme, Clermont-Ferrand, France

Abstract. Recently, deglaciated landscapes are ideal natural arenas to investigate ecological succession processes. However, ground data acquisition remains complicated as glacier forefields are often difficult to access and fieldwork possibilities remain limited. Remote sensing offers an opportunity to bypass this issue and increase spatial and temporal coverage of ecological parameters. The Landsat satellites (5 to 8) provide reflectance data for the past 40 years, which align with recent phenomena of glacier retreat and related ecological and geomorphological dynamics in glacier forefields. Difficulties remain as information retrieved from 30-m Landsat pixels are the result of a mixture of objects influencing reflectance signals. Here, we used a submeter multispectral unmanned aerial vehicle (UAV) image of the *Glacier noir* foreland, France, to assess the sensitivity of Landsat normalized difference vegetation index (NDVI) to subpixel vegetation and topographic components. We found a twofold linear relationship ($a = 0.456$) and high sensitivity between fractional vegetation cover (FVC) and Landsat NDVI with detection of low vegetation changes (FVC > 5%) at low NDVI values (<0.1) (F-score = 0.75). We also showed that vegetation height and subpixel topographic heterogeneity leads to misestimation of vegetation cover as quantified by Landsat NDVI. Overall, our comparative analysis using very-high resolution UAV imagery provides support for the use of widely available Landsat imagery for investigating vegetation dynamics in glacier forefields.
 [DOI: 10.1117/1.JRS.15.044508]

Keywords: glacier forefields; Landsat; normalized difference vegetation index; unmanned aerial vehicle; sensitivity; topography.

Paper 210514 received Aug. 12, 2021; accepted for publication Oct. 18, 2021; published online Nov. 1, 2021.

1 Introduction

Since the end of the Little Ice Age in the Alps[1,2] (~AD 1850), glaciers have decreased in size and volume[3] and their fronts have retreated providing new open surfaces for primary vegetation succession to occur. The extent of glaciers in the French Alps, for example, has decreased by roughly 50% since the mid-19th century, with a pronounced acceleration in glacier retreat since the 1980s due to the global climate warming of roughly 0.5°C per decade.[4,5] Recently, deglaciated areas (glacier forefields, hereafter) are characterized by strong interactions between vegetation dynamics and geomorphological processes and landforms.[6–10] Vegetation tends to colonize the new open areas and may enhance landform stabilization, but at the same time

*Address all correspondence to Arthur Bayle, arthur.bayle.env@gmail.com

1931-3195/2021/$28.00 © 2021 SPIE

in these fresh open areas, geomorphological processes (e.g., debris flow, gullying, interrill erosion, frost creep, and solifluction) can rapidly change in quality and intensity, impacting landform stability and vegetation succession trajectories.[11] In this context, glacier forefields are ideal models for investigating reciprocal interactions between vegetation succession and geomorphological processes in a dynamic and changing environment subjected to global warming.[12]

Vegetation succession stage depends on autogenic processes that are a function of time since deglaciation.[13,14] However, glacier forefields are constantly impacted by geomorphological disturbances that enhance the formation of a dynamic and heterogeneous mosaic of habitats and vegetation units. Recent studies indicate that successional trajectories and their rate and turnover within glacier forefield are also controlled by allogenic geomorphological processes (mixture of hillslope, torrential, and periglacial processes).[15–21] Wojcik et al. suggested that the complex interplay between autogenic and allogenic components varies over time, with an initial stochastic phase followed by a more deterministic phase defined by environmental factors and biogeomorphological feedbacks. In addition, variability in plant succession rates has been linked to elevation gradients with, e.g., warmer low-elevation glacier forefields that tend to evolve faster from pioneer vegetation to taller birch woodland than colder high-alpine glacier forefields.[22]

In situ investigation of vegetation succession in mountainous areas requires considerable human effort and cost, given that data must be collected from contrasting glaciological, geomorphological, and vegetation contexts within the glacier forefield. Fieldwork campaigns in poorly accessible sites are often "one-shot" studies, and analyses of vegetation succession thus remain limited to a space-for-time approach.[23] Furthermore, traditional ecological field campaigns in the Alps often tend to focus on stable vegetated surfaces and ignore disturbed and unstable zones where vegetation is absent or has a low cover.[22,24] However, the consideration of these unstable areas with low or patchy pioneer vegetation cover is necessary for a better understanding of the initial conditions that control vegetation establishment and subsequent successional trajectories.

Remote sensing data provide great potential for analyzing Earth's surface dynamics at various spatiotemporal scales, particularly in areas that are challenging to access.[25] More specifically, the repeat survey capabilities (i.e., 16-day) and the spatial resolution of the Landsat satellites (i.e., 30 m) allow for observation of vegetation colonization dynamics in the wake of glacier retreat using a near real-time approach.[11,19,26] Acquisition of normalized satellite images began in 1984 with Landsat 5 TM and has continued with the Landsat 7 ETM+ and Landsat 8 OLI sensors, both of which are still operating. With almost 40 years of data acquisition, the historical depth of monitoring is consistent with the rapid glacier retreat that has occurred since the 1980s all around the world in mountainous ranges.[27] Historical archives of optical satellite imagery provide a unique opportunity to simultaneously observe deglaciation dynamics[28] and related primary vegetation succession using appropriate vegetation indices, such as the normalized difference vegetation index (NDVI). NDVI can be defined as a nonphysical unidimensional quantity sensitive to certain physical properties of the vegetation canopy, notably biomass, and photosynthetic activity.[29] However, in the context of glacier forefields, Landsat pixels with a resolution of 30 m are expected to be composed of a mixture of diverse ground features (e.g., type of rock, soil, and vegetation; slope and roughness) with unique moisture and reflectance properties with unquantified consequences for NDVI values.

A mixed pixel (mixel) is a picture element representing an area occupied by more than one entity of interest or by one single entity of interest but with difference in bidirectional reflectance distribution function, e.g., a homogeneous grassland visible on both sides of a crest or a flat grassland with sparse trees.[30] Glacier forefields are unstable, and extremely heterogeneous environments composed exclusively of mixels at Landsat scale. Therefore, ability to interpret observations of changes in vegetation following deglaciation using Landsat imagery first and foremost requires identifying the dependency between NDVI and reflectance-contributive features.

Here, we assess the relationship between Landsat NDVI and ground vegetation in a glacier forefield by deriving submeter variables from unmanned aerial vehicle (UAV) imagery. Due to bidirectional acquisition and very-high resolution, UAV-based approach allows to extract an ensemble of variables that informs us on the topographic and vegetation structure that are unapproachable through coarse resolution sensors. Using subpixel information on orientation, slope, fractional vegetation cover (FVC), and vegetation height, we address the following questions:

(i) what vegetation changes can we expect on the ground for a given variation in Landsat NDVI; (ii) at which value of NDVI can we consider a Landsat pixel as vegetated; and (iii) what vegetation and topographic components impact the relation between Landsat NDVI and vegetation on the ground? Addressing these methodological questions is crucial prior to applying the entire Landsat archive toward assessment of vegetation dynamics following deglaciation, and more specifically tackling the questions of lag between deglaciation and vegetation colonization, and spatiotemporal variability of successional trajectories.

2 Material and Methods

2.1 *Glacier Noir Foreland*

The *Glacier Noir* is located in the *Haute Vallée de St. Pierre* in the Ecrins National Park in the French Alps (Fig. 1). It is a 4.5-km long debris-covered glacier with an elevation range from 2200 to 3600 m. Its tongue is oriented east, pouring out in the *Pré de Madame Carle* field. The *Glacier Noir* forefield consists of a complex assemblage of hummocky moraines and fluvioglacial landscape units resulting from debris cover and changes in glacier extent and thickness since the LIA. Indeed, the thick supraglacial debris over the *Glacier Noir* induces longer response time to climate fluctuations, and changes in its front position are not always synchronous with those of its neighbor, the *Glacier Blanc*.[31,32] Two contrasting proglacial landscapes can be distinguished: (i) the downstream part of the glacier forefield, from the LIA moraines to the 1950s moraines,[33] which is covered by shrubs and trees, and (ii) the upstream part, situated between the 1950s moraines and the current glacier front, which is sparsely vegetated by narrow and isolated patches of alpine herbs.

2.2 *Data Acquisition*

2.2.1 *UAV imagery*

On the morning of September 15, 2020, we used a quadcopter UAV (microdrones® md4-1000) to fly over the glacier forefield of the *Glacier Noir*. The UAV carried a multispectral camera (Micasense Rededge) and over the course of four collected images composed of five spectral bands (i.e., blue, green, red, red-edge, and near-infrared) of the complete glacier forefield area (Table 1). Previously, a set of 16 photogrammetry targets were placed over the entire proglacial area and georeferenced in Lambert 93 using a trimble R10 DGPS. Images were then orthorectified using the common Agisoft metashape workflow,[34,35] allowing us to generate an RGB

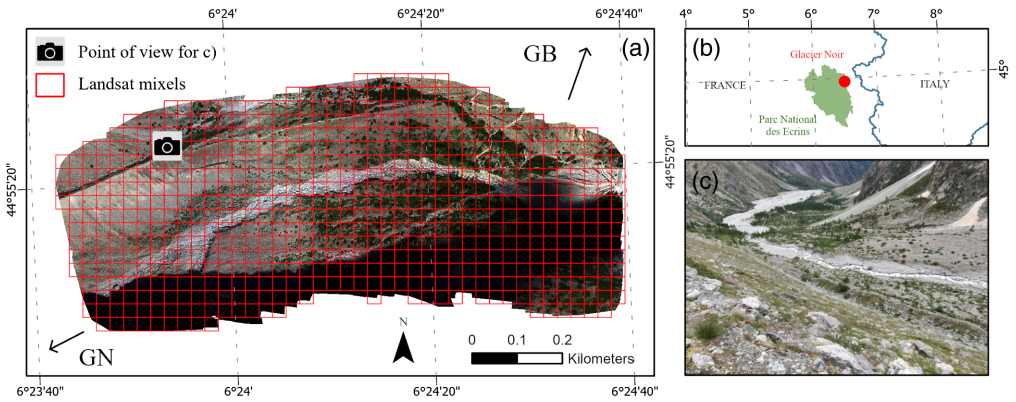

Fig. 1 (b) *Glacier Noir* foreland located in the *Parc National des Ecrins*, France, observed by (a) RGB image from UAV acquisition. Landsat mixels considered in this study are shown as a red grid. (a) Directions of *Glacier Noir* and *Glacier Blanc* are indicated with arrows. Point of view for (c) is located in (a).

Table 1 Band wavelengths and spatial resolution of the Red and NIR bands from the UAV and OLI sensors.

Sensor	Red band	NIR band	Resolution
UAV	668 ± 14 nm	842 ± 57 nm	12 cm
OLI	655 ± 25 nm	865 ± 20 nm	30 m

orthomosaic, NDVI layer, digital surface model (DSM), and digital elevation model (DEM) at a resolution of 12 cm with an RMS error of 1.4 cm in XY and 2.2 cm in Z. The DEM raster was produced using the dense cloud filtering and classification methods available in Agisoft Metashape Professional (1.7.3).

2.2.2 *Landsat reflectance and NDVI*

Landsat 8 OLI standard terrain-corrected orthorectified images from collection 2 from September 3, 2020, and September 28, 2020, were downloaded from the Landsat Earth Explorer data portal at surface reflectance level of correction. These scenes were chosen as they are cloud-free over *Glacier Noir* forefields, and their mean reflectance are expected to be close to the UAV reflectance. The scene from September 12, 2020, could not be used due to cloud cover. Topographic-related effects were not corrected using available methods[36] as we subsequently measured the impact of these effects through geomorphological variables on NDVI Landsat mixel values.

NDVI was computed for the two scenes using the red and near-infrared bands according to the following equation, where NIR and Red corresponds to the reflectance measures in bands 5 (0.85 to 0.88 nm) and 4 (0.64 to 0.67 nm) of Landsat 8 OLI sensor (Table 1), respectively:

$$\mathrm{NDVI} = \frac{(\mathrm{NIR} - \mathrm{Red})}{(\mathrm{NIR} + \mathrm{Red})}. \tag{1}$$

The NDVI mean of the two scenes was computed and used as the explanatory variable for further analysis, hereafter referred as NDVI Landsat mixel.

2.3 *Preparation of Vegetation and Topographic Data*

2.3.1 *Shadow masking*

Shadows in remote-sensing images decrease the quality of spectral information and hamper processes, such as feature extraction and classification.[37,38] In mountainous contexts, illumination conditions depend mostly on slope orientation and angle and large obstructing topographic features. Here, we intend to mask shadows that completely obstruct illumination, given that we are interested in the effects of topographic heterogeneity within a mixel. Many methods have been proposed ranging from simple property-based methods relying on combining spectral bands and thresholding to geometry and physics-based methods accounting for surrounding topography and atmospheric conditions. Because our study case is relatively simple due to the surface considered and the very high resolution, we generated a mask by applying a threshold to the NIR band. Histogram thresholding is the simplest shadow detection tool as it assumes that there is a clear separation between shadow and sunlit histogram levels. A common limitation is the confusion between water bodies and shadows, but as we solely focused on vegetation, this issue was not relevant. Since the NIR band is more sensitive to shadows, it was chosen over RGB channels for histogram thresholding [Fig. 2(a)]. We manually selected a threshold of 0.07 leading to the removal of 38 % of the image [example in Figs. 2(b) and 2(c)].

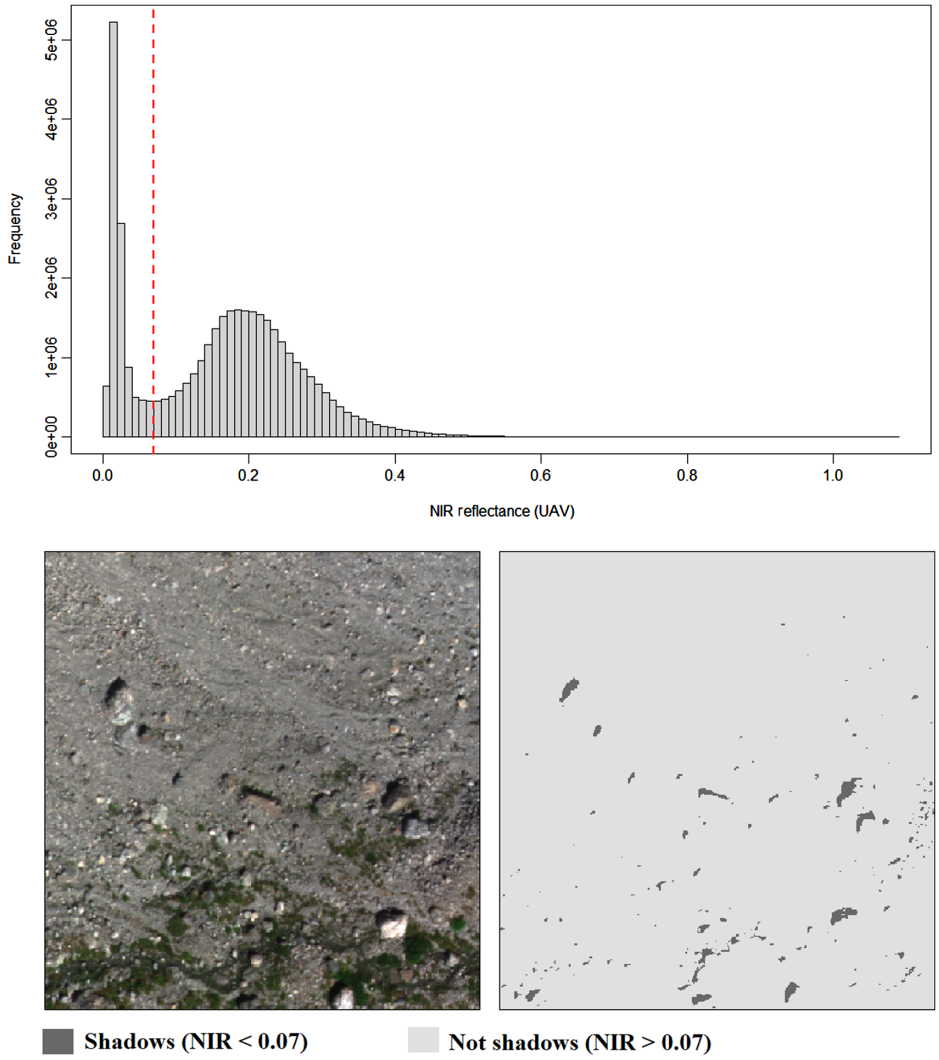

Fig. 2 (a) Bimodal histogram of the NIR band derived from the UAV acquisition with the threshold of 0.07 in red dashed line to distinguish shadowed pixels from nonshadowed pixels. (b), (c) An example of shadows masking results.

2.3.2 *Vegetation cover*

We derived a binary mask of vegetated versus unvegetated pixels from UAV images by photointerpreting ground truth samples of vegetation and bare surfaces for binary classification based on NDVI. First, we masked pixels identified as shadows. Then, we photointerpreted 820 and 894 samples of vegetation and bare soil from the 12-cm RGB image, respectively. Based on these samples, we derived NDVI distribution for both classes and computed the confusion matrix based on a moving threshold. We computed F-score, which is the harmonic mean of recall (fraction of correctly classified pixels with regard to validation samples) and precision (fraction of correctly classified pixels with regard to all pixels classified as such in the image), for all thresholds using the following equation:

$$F\text{-score} = 2 * \frac{\text{Precision} * \text{Recall}}{\text{Precision} + \text{Recall}}, \tag{2}$$

$$\text{Precision} = \frac{\text{TP}}{\text{TP} + \text{FP}}, \tag{3}$$

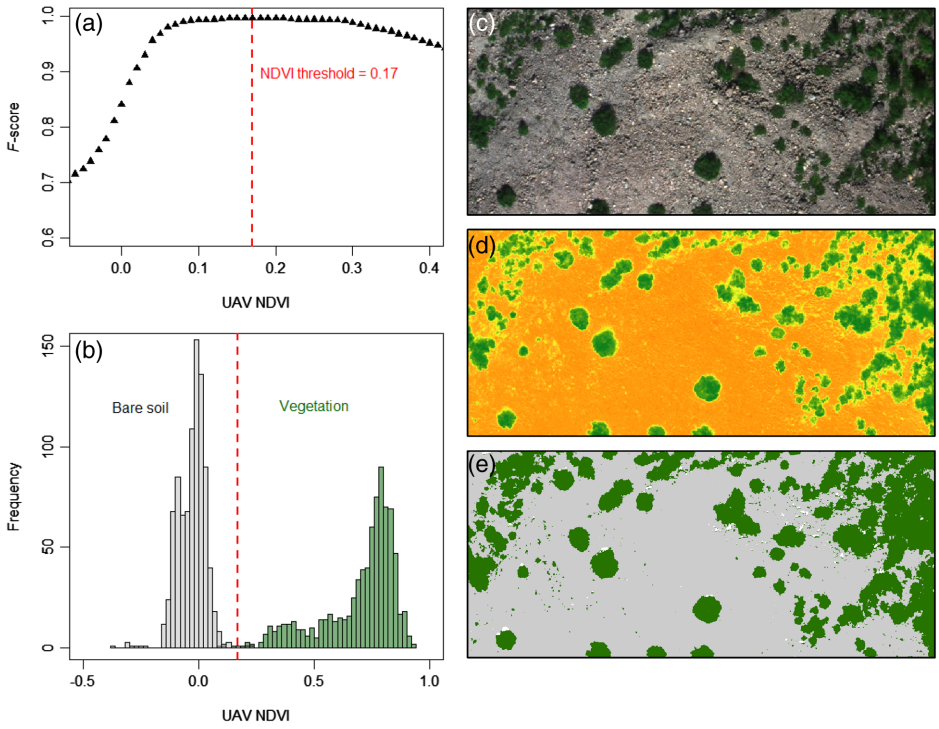

Fig. 3 (a) *F*-score distribution along a UAV NDVI gradient used as threshold to distinguish vegetation from bare soil based on the photointerpreted samples. (b) Distribution of UAV pixels for bare soil (gray) and vegetation (green) along a UAV NDVI gradient. (a), (b) The retained threshold is shown by the red vertical dashed line. Example of (a) an RGB images, (d) NDVI, and (e) the classification as vegetation or bare soil using an NDVI threshold of 0.17.

$$\text{Recall} = \frac{\text{TP}}{\text{TP} + \text{FN}}, \tag{4}$$

where TP is the true positive, TN is the true negative, FP is the false positive, and FN is the false negative. We selected the NDVI value that maximized the *F*-score. The value scoring an *F*-score of 0.99 gives an NDVI threshold of 0.17 [Fig. 3(a)]. We obtained very high *F*-score (>0.95) for NDVI ranging from 0.08 to 0.28 [Fig. 3(a)], which is justified by the very high resolution of the UAV image and our pixel-based approach. NDVI variation between 0.08 and 0.28 corresponds to pixels transitioning from vegetation patches to bare soil, thus leading to large range to discriminate both classes [Figs. 3(b)–3(e)].

2.3.3 *Vegetation height and topographic variables*

The vegetation height model was computed as the subtraction of the DEM from the DSM previously produced using UAV images. Slope and aspect were obtained from the DEM using SAGA GIS 7.3[39] at the coarser scale of 1-m pixel resolution. We transformed the circular aspect to the linear topographic solar radiation aspect index (TRASP) using the following equation:

$$\text{TRASP} = \frac{\left[1 - \cos\left(\frac{\pi/180}{a-30}\right)\right]}{2}, \tag{5}$$

where a is the aspect in degrees that gives a value of 1 on the hotter, dryer, south–south–westerly slopes and 0 to land oriented in a north–northeast direction.[40] Finally, a statistical summary (mean and standard deviation) of vegetation height, slope, and TRASP were computed for each landsat mixel/pixel using the zonal statistics tools available within ArcGIS 10.5 (Fig. 4).

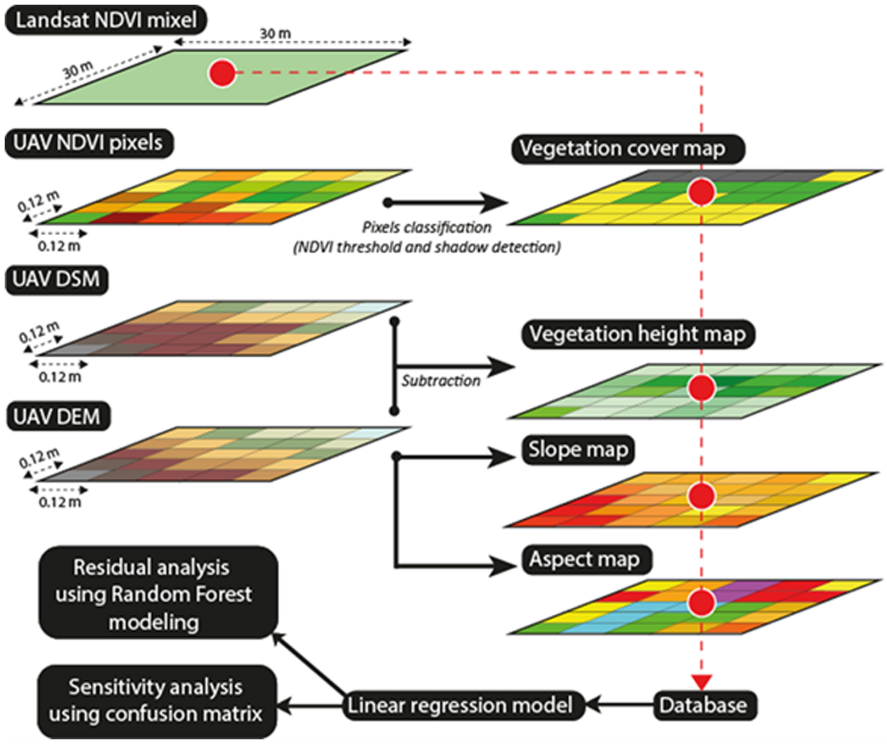

Fig. 4 Methodological workflow of the analysis.

2.4 *Statistical Analysis*

To assess the relationship between Landsat NDVI and ground vegetation, we computed a linear model between Landsat NDVI and FVC estimated using NDVI UAV pixels. The adjusted-R^2 was calculated to measure the quality of the prediction. From this relationship, we carried out two independent analyses presented in Fig. 4.

First, we considered mixels as nonvegetated if the percentage of vegetation cover were inferior to 5%, which would mean 1.5 m^2 of vegetation within a 30-m^2 pixel. We then computed confusion matrices based on a moving threshold of Landsat NDVI to best split vegetated and nonvegetated mixels. The NDVI threshold achieving the maximum F-score was considered as the best value to statistically consider a pixel as containing vegetation or not. Optimal threshold is presented by showing the distribution of recall and true negative rate (TNR) along Landsat NDVI. TNR was computed as follows:

$$\mathrm{TNR} = \frac{\mathrm{TN}}{\mathrm{TN} + \mathrm{FP}}. \tag{6}$$

Second, we implemented a random forest classification analysis to assess relationships between the linear model residuals and predictors.[41] We classified the residuals into three categories: negative residuals (Res < -0.025), null residuals ($-0.025 <$ Res < 0.025), and positive residuals (Res > 0.025). The threshold of 0.025 was chosen to equalize the number of pixels in each class, resulting in 89, 83, and 74 samples for negative, null, and positive residuals. Only 74 samples were conserved for each class. Predictor variables included mean vegetation height, mean TRASP, mean slope, TRASP standard deviation, and slope standard deviation. These variables were chosen to first represent the vegetation structure (mean vegetation height) and second to represent the topographic context (mean TRASP and slope) and the within-mixel topographic variability (standard-deviation of TRASP and slope). We screened collinear variables by running a multicollinearity test ($a = 0.05$). No variables were discarded due to multicollinearity. Next, we randomly partitioned the data set into sets for model training (two-third) and evaluation (one-third), and then repeatedly fit random forest models to optimize out-of-bag classification

accuracy. We reassessed the classification accuracy using the data withheld for model evaluation. Lastly, we computed predictor importance using the mean decrease in accuracy metric. Predictor importance was based on a permutation-based importance measure where one measures the effect of reshuffling each predictor on model accuracy. Finally, we generated partial dependence plots to assess how class-specific classification probabilities varied across the range of each predictor while holding all other predictors at their average value. The distribution of predictors values distribution is shown on each plot, given that partial dependencies plots tend to overinterpret regions even with almost no data. Thus, curves should be interpreted only in regions covered by initial data. We used the randomForest, caret, and pdp R packages to implement random forest models and evaluate their performance.[42,43]

3 Results

3.1 *Relation between Landsat NDVI and Vegetation Cover*

The relation between NDVI derived from Landsat and FVC derived from UAV imagery is linear with an increase of 10% in surface covered by vegetation approximately leading to an increase in NDVI of 0.05 (Fig. 5). The model showed an adjusted-R^2 of 0.7 and a p-value < 0.001. Starting from ~80% of FCV, residuals tended to be mostly positive and vegetation height higher suggesting the beginning of an asymptotic phase in which NDVI increases quickly with increasing FCV.

3.2 *Sensitivity of Landsat NDVI to Presence of Vegetation*

Mixels were considered as vegetated when the percentage of surface covered by vegetation was above 5%. Considering this threshold, 41 and 205 mixels were assigned as not vegetated and

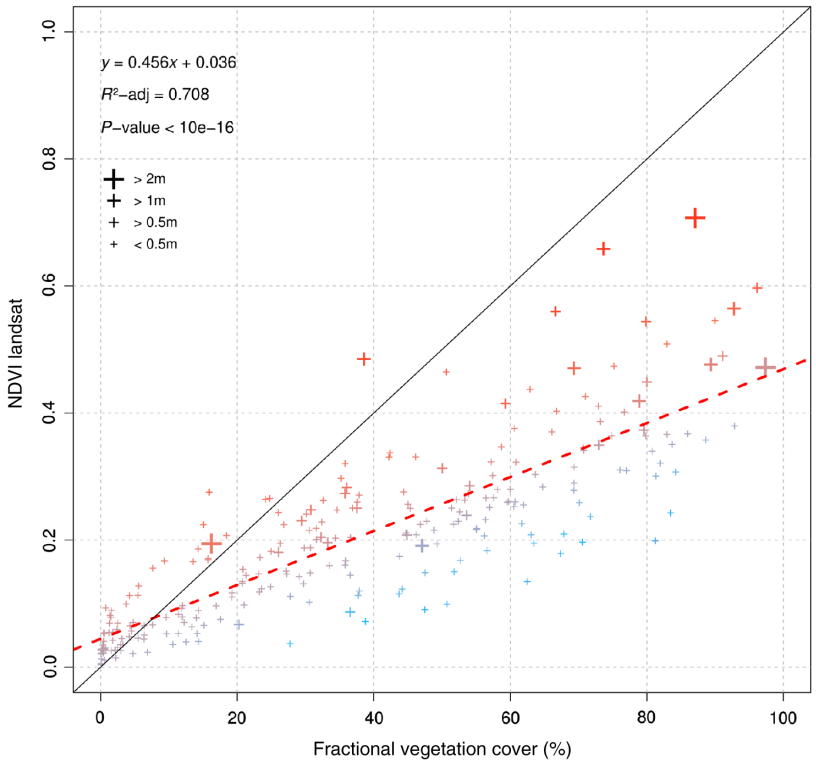

Fig. 5 Relationship between Landsat NDVI and percentage of surface covered by vegetation derived from UAV NDVI. The linear model is shown by a red dashed line and colored points represent residuals from the linear model with red and blue showing positive and negative residuals, respectively. Cross size indicates the mean vegetation height of the mixel.

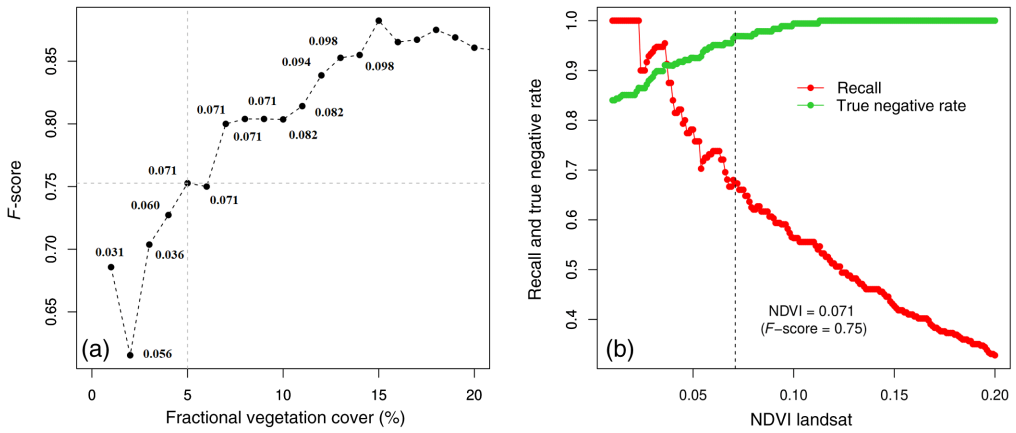

Fig. 6 (a) Distribution of best *F*-score and corresponding Landsat NDVI values obtained to discriminate between more and less than *X*% of FVC. (b) Distribution of recall and TNR along the Landsat NDVI threshold gradient used to discriminate between mixels with more and less than 5% of FVC. The vertical dashed line corresponds to the NDVI threshold chosen to maximize the *F*-score.

vegetated, respectively. The confusion matrix was computed for NDVI Landsat from 0.01 to 0.2 to find the NDVI threshold resulting in the highest *F*-score. The best model achieved an *F*-score of 0.75 resulting in an NDVI threshold of 0.071. Recall and TNR were 0.67 and 0.96, respectively, meaning that we tend to consider 33% of the vegetated mixels as unvegetated. This procedure was repeated for FVC ranging from 0 to 20, which showed the higher *F*-score for an FVC superior to 15% [Fig. 6(a)].

3.3 *Within-Pixel Vegetation Structure and Topographic Context*

The random forest model achieved an overall accuracy of 62%, which translated a good capacity of the five predictors to classify residuals as positive, null, or negative. Decrease in accuracy was used to order the five predictors according to their importance for overall classification accuracy and relative to classification accuracy for each class (Fig. 7).

The TRASP, slope, and vegetation height mean were overall the most important predictors of the random forest [0.04, 0.021, and 0.027, respectively; Fig. 7(a)] and for the negative and positive residuals classes [Figs. 7(b) and 7(c)] while slope mean was the most important predictor for null residuals [Fig. 7(d)]. Null residuals seem to occur more often on homogeneous (TRASP SD < 0.17) steep slopes (>32 deg) and in lower vegetation height (mean height < 0.15 cm). Positive residuals seem to occur more often in south-oriented (TRASP > 0.6) flat slope (<17 deg) and with higher vegetation (mean height > 50 cm), whereas negative residuals seem to occur more often in north-oriented (TRASP < 0.3) moderate slope (17 deg < slope < 32 deg) and less likely with higher vegetation (mean height > 50 cm) (Fig. 8).

4 Discussion

While most deglaciation datasets are based on remote sensing observations,[4] the analysis of vegetation succession still relies mostly on fieldwork in a space-for-time framework and without the precious addition of historical remote sensing methods, with exceptions.[8,11,19,26] Nonetheless, challenges remain in the search for an optimal and reliable relationship between remotely detected changes in vegetation indices, such as NDVI, and actual vegetation changes on ground.

The correspondence between NDVI and certain biophysical properties of the vegetation canopy, such as leaf area index (LAI), FVC, vegetation condition, and biomass, has been widely studied.[44–48] Overall, it has been shown that NDVI increases near-linearly with FVC (horizontal density) until values reach between 80% and 90%, at which point it tends to saturate and increase very slowly with increasing LAI (vertical density).[49–53] Using a combination of 30×30 m^2 Landsat NDVI data and 12×12 cm^2 UAV NDVI to derive horizontal and vertical vegetation

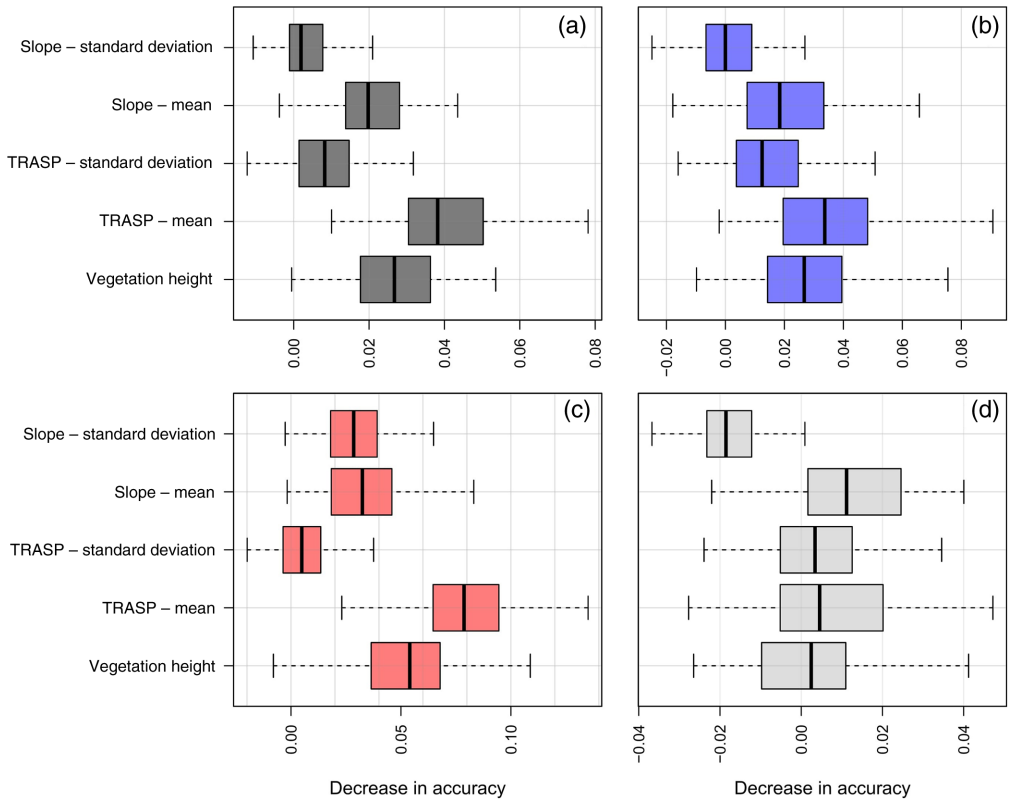

Fig. 7 Variable importance as decrease in accuracy from (a) the random forest model considering the three classes, (b) the negative residuals only, (c) the positive residuals only, and (d) the null residuals only.

density, we found similar results with a twofold linear relationship between FVC and NDVI, which tends to deteriorate at higher FVC due to vegetation height (Fig. 5). In the specific case of recently deglaciated areas colonized by vegetation, if we know the year of deglaciation, we are certain of the absence of vegetation at initial stage. Thus, our ability to detect the turning point when productivity rises and vegetation succession begins is key for understanding the complex biogeomorphological feedbacks in glacier forefields.

We found that an NDVI value of ∼0.07 was optimal to distinguish Landsat pixels with more or less than 5% FVC (Fig. 6). The confidence in discrimination efficacity tends to increase from 0% of FVC to 15% [Fig. 6(a)], where it shows the best F-score for low vegetated Landsat pixels. Considering an NDVI value of 0.071, we still miss 33% of pixels with FVC superior to 5%. Sensitivity of Landsat imagery to absence/presence of vegetation is mostly analyzed in post-disturbance contexts, e.g., following fire[54] or landslides.[55] Nonetheless, most of these systems are not applicable to glacier forefields as they are not defined as primary succession. On average, Landsat 8 NDVI values of 0.3 and 0.2 are observed post-fire and landslide, respectively[55] Recent work in the Antarctic provides a more comparable context to that of alpine glacier forefields, with a gradient from bare soil to very sparse vegetation. In agreement with our results, Fretwell et al (2011)[56] found that, using Landsat ETM one the Antarctic Peninsula, NDVI values between 0.05 and 0.1 mostly corresponded to vegetated areas (∼70%), whereas only ∼20% of pixels with NDVI values under 0.05 were vegetated. In a similar context, Sotille et al.[57] found that higher NDVI values around 0.1 are required to effectively discriminate vegetation using Landsat 8 using UAV data as validation. Overall, our results, supported by other studies, showed that Landsat is sensitive to very sparse vegetation considering that we found consistent results for around 5% of FVC, which corresponds to 1.5 m^2 of vegetation within a 30-m^2 pixel (F-score = 0.75).

Variability in NDVI responses to FVC may come from various sources and with nonlinear influence along the FVC gradient. The lower the FVC is, the more we are accounting for soil reflectance properties in red and NIR bands.[58] Whereas at high FVC, the relationship will be

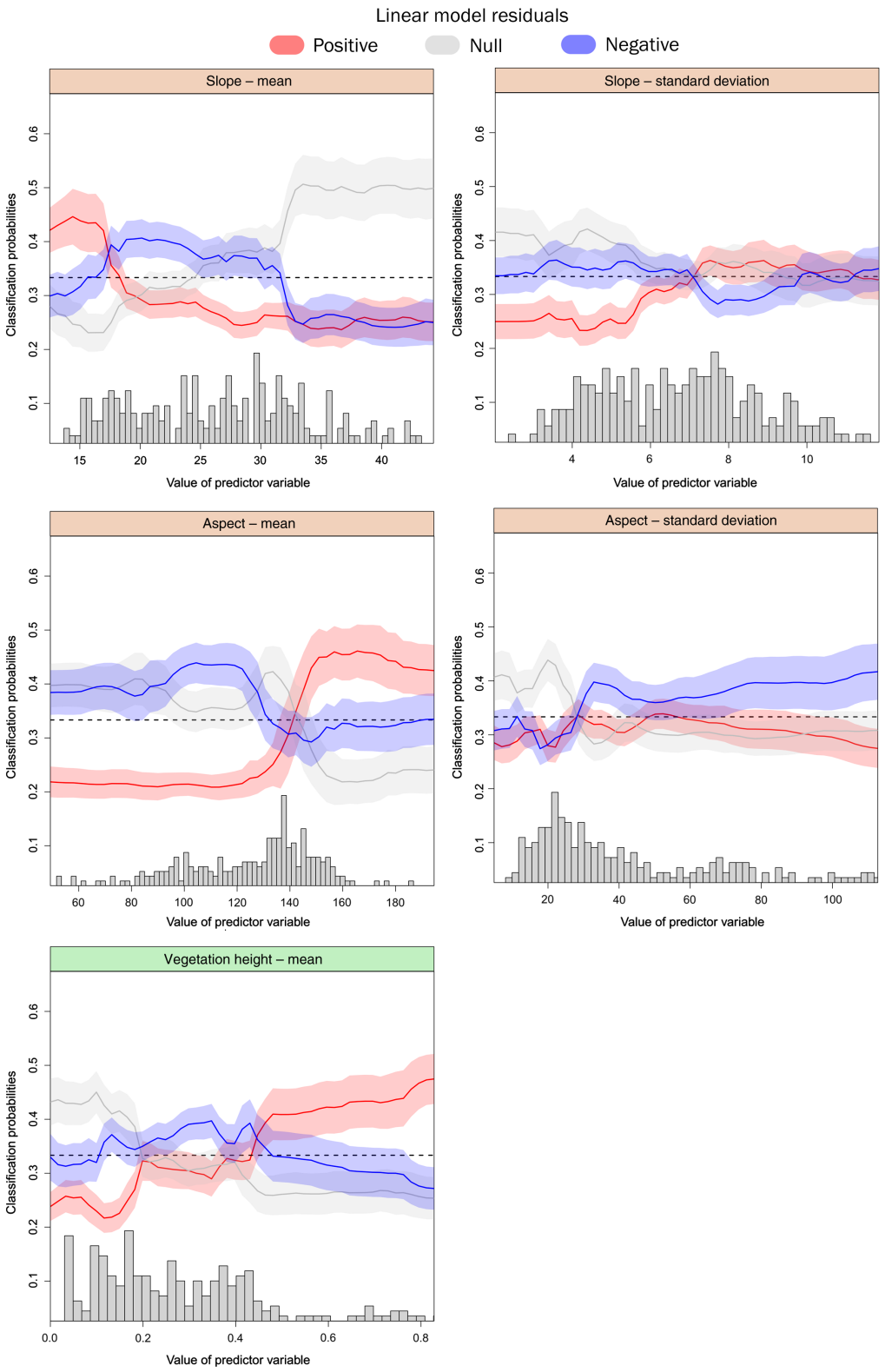

Fig. 8 Partial dependency plots illustrating how each predictor variable affects class probability while accounting for the mean effect of other predictors in the model. Error bands depict the standard deviation from the 10 run of random forest with randomization in the samples used for training and evaluation. Histogram shows the data distribution to avoid interpretation of values range with few or no data.

mostly affected by vegetation structure.[51] Through the investigation of vegetation structure (height) and topographic context (TRASP and slope) influence on NDVI ~ FVC model residuals, we showed that Landsat NDVI values tend to be higher than expected for a given value of FVC in the case of south-facing slopes and higher vegetation height, whereas values tend to be lower in the context of north-facing slopes and lower vegetation height (Figs. 5 and 8). As expected, the relationship is neutral in the case of homogeneous slope angle and orientation with low vegetation height (Figs. 7 and 8). Accordingly, we showed that the variability of NDVI values along a gradient of vegetation cover is dependent on vegetation structure and topography in the context of the *Glacier Noir* forefield. That means that topographic heterogeneity reduces the sensitivity of Landsat NDVI to sparse vegetation. We did not account for factors such as soil moisture and texture, despite the well-known effects on soil reflectance,[58] as ground measures are complex and expensive to acquire in the context of glacier forefields.

Further studies could benefit from methods such as global navigation satellite systems reflectometry to improve our understanding of *in situ* soil moisture influence on NDVI response to FVC.[59,60] In addition, while we account for vegetation structure through height, we did not account for vegetation type, which has been shown to be determinant in the NDVI signal.[56] For example, spectral response of Antarctic vegetation species in the NIR region is known to vary between vascular plants and lichens.[61,62] Vegetation composition could also affect NDVI values in glacier forefields due to the presence of contrasting plant functional groups and high diversity.[63]

While deriving vegetation maps from very-high resolution UAV data does not correspond to exhaustive ground-truth mapping of vegetation, it offers an efficient solution for generating spatially continuous maps of FVC for sites where fieldwork would be extremely time-consuming and potentially dangerous. We considered that the extremely high spatial resolution offered by UAV-acquired imagery provided a "ground truth" quality layer with respect to Landsat imagery. Nonetheless, true fieldwork data, coupled with hyperspectral imagery,[64] would still be needed to further investigate the effects of soil properties and vegetation type on Landsat NDVI values.

Despite the lack of consideration of certain factors discussed above, we are confident that our work is a step forward toward understanding how remote sensing methods can improve the quantification of primary succession dynamics following deglaciation. In contrast to the classical approach, which relies on the key assumption that all sites within a glacier forefield only differ with respect to time since deglaciation, a biogeomorphological approach takes into account feedbacks between ecological and geomorphological processes in the analysis of vegetation dynamics and trajectories of succession in glacier forefields.[65,66] Biogeomorphological studies have shown that landscape dynamics within glacier forefields depend on the balance between stabilizing and destructive forces.[66] Substrate stabilization occurs where vegetation reaches their window of opportunity and feedback window. Destruction is controlled by geomorphological disturbances that are defined as the geomorphological events that causes a modification in the structure of the ecosystem and drives changes in the physical environment.[65,67,68] Thus, biogeomorphological studies in the glacier forefield context require accurate and spatially continuous determination of (1) the time between the onset of ice-free conditions and the beginning of surface colonization by plants to assess time-lag and (2) the time-series of vegetation growth and potential disturbance following establishment. Observed vegetation dynamics could thus be overlaid with geomorphological layers to assess spatial and temporal covariation between plant succession and biogeomorphic processes. Comparative analysis between glacier forefields underscores the need to test the transposability of our method to other glacier forefields with various topographic and ecological conditions.

As similar results in terms of Landsat sensitivity to vegetation cover were found in other contexts,[56] we are confident that our analysis is relevant for other glacier forefields. Indeed, the common features observed in these cryoecosystems are the abundance of large granules[69] and oligotrophic soils,[70,71] which are both crucial elements driving pixel-scale soil reflectance. Furthermore, we showed that, while there is a topographic effect in terms of slope angle and orientation on NDVI response to vegetation cover, it is minor and significant impacts can be expected only for large latitudinal gradients or with opposite slopes within the same forefield. In both cases, several methods are available to correct for these effects in the case of Landsat images and have been applied with good results in other contexts.[36,72]

5 Conclusion

Primary succession patterns occurring in glacier forefields following deglaciation are complex processes occurring in highly heterogeneous environments. *In situ* and comprehensive investigation of this heterogeneity/spatial variability remains difficult due to often dangerous access and the high human effort and cost required. Furthermore, initial conditions and plant community responses following deglaciation are often unknown at the time of fieldwork, which constitutes an inherent shortcoming of the space-for-time approach. Remote sensing data, and more specifically Landsat, provide reflectance measurements at relatively fine spatial resolution and with decadal-scale historical depth, which could allow for investigation of within glacier forefield heterogeneity of vegetation dynamics over the past 35 years. However, issues remain in the understanding of Landsat NDVI sensitivity to low changes in vegetation structure (horizontal and vertical density) and the impact of topography and substrate on these relationships. Here, we took a step forward to investigate these concerns. We demonstrated that incremental changes in NDVI at low values efficiently track small changes in FVC at low values, which typically correspond to pioneer vegetation in glacier forefields. We also showed that vegetation height and topography affect the relationship between fractional plant cover and NDVI, and thus should be considered when interpreting ecological succession patterns using Landsat NDVI. Overall, our results provide support for the use of the Landsat time series to assess the timing and rate of plant colonization following deglaciation.

Acknowledgments

No potential conflict of interest was reported by the authors.

Code, Data, and Materials Availability

The data that support the findings of this study are available from the corresponding author, A.B., upon reasonable request.

References

1. J. A. Matthews and K. R. Briffa, "The 'Little Ice Age': re-evaluation of an evolving concept," *Geogr. Ann.* **87**(1), 17–36 (2005).
2. M. Gardent, "Inventaire et retrait des glaciers dans les alpes françaises depuis la fin du Petit âge glaciaire," PhD dissertation, Université de Grenoble, Grenoble, France (2014).
3. R. Hock et al., "GlacierMIP—a model intercompaison of global-scale glacier mass-balance models and projections," *J. Glaciol.* **65**(251), 453–467 (2019).
4. M. Gardent et al., "Multitemporal glacier inventory of the French Alps from the late 1960s to the late 2000s," *Glob. Planet. Change* **120**, 24–37 (2014).
5. A. Gobiet et al., "21st century climate change in the European Alps: a review," *Sci. Total Environ.* **493**, 1138–1151 (2014).
6. C. A. Burga et al., "Plant succession and soil development on the foreland of the Morteratsch glacier (Pontresina, Switzerland): straight forward or chaotic?" *Flora* **205**(9), 561–576 (2010).
7. J. Eichel et al., "Biogeomorphic interactions in the Turtmann glacier forefield, Switzerland," *Geomorphology* **201**(1), 98–110 (2013).
8. A. J. A. M. Temme and K. Lange, "Pro-glacial soil variability and geomorphic activity: the case of three Swiss valleys," *Earth Surf. Process. Landf.* **39**(11), 1492–1499 (2014).
9. T. Heckmann, S. McColl, and D. Morche, "Retreating ice: research in pro-glacial areas matters," *Earth Surf. Process. Landforms* **41**, 271–276 (2016).
10. H. R. Miller and S. N. Lane, "Biogeomorphic feedbacks and the ecosystem engineering of recently deglaciated terrain," *Prog. Phys. Geogr.* **43**, 24–45 (2019).
11. M. J. Klaar et al., "Vegetation succession in deglaciated landscapes: implications for sediment and landscape stability," *Earth Surf. Process. Landforms* **40**, 1088–1100 (2015).

12. J. Eichel, "Vegetation succession and Biogeomorphic Interactions in glacier forelands," in T. Heckmann and D. Morche, Eds., *Geomorphology of Proglacial Systems*, pp. 327–249, Springer, Cham (2019).
13. L. R. Walker et al., "The use of chronosequences in studies of ecological succession and soil development," *J. Ecol.* **98**, 725–736 (2010).
14. K. Rydgren et al., "Glacier foreland succession and the fading effect of terrain age," *J. Veg. Sci.* **25**(6), 1367–1380 (2014).
15. J. A. Matthews, "Disturbance regimes and ecosystem response on recently-deglaciated substrates," *Ecosystems of the World*, pp. 17–38 (1999).
16. M. Moreau et al., "Impacts of recent paraglacial dynamics on plant colonization: a case study on Midtre Lovénbreen foreland, Spitsbergen (79 N)," *Geomorphology* **95**, 48–60 (2008).
17. J. Eichel, D. Corenblit, and R. Dikau, "Conditions for feedbacks between geomorphic and vegetation dynamics on lateral moraine slopes: a biogeomorphic feedback window," *Earth Surf. Process. Landforms* **41**(3), 406–419 (2016).
18. R. Wojcik et al., "Time since deglaciation and geomorphological disturbances determine the patterns of geochemical, mineralogical and microbial successions in an Icelandic foreland," *Geoderma* **379**, 114578 (2020).
19. A. Bayle, "A recent history of deglaciation and vegetation establishment in a contrasted geomorphological context, Glacier Blanc, French Alps," *J. Maps* **16**(2), 766–775 (2020).
20. J. D. Phillips and P. Šamonil, "Biogeomorphological domination of forest landscapes: an example from the Šumava Mountains, Czech Republic," *Geomorphology* **383**(15), 107698 (2021).
21. R. Wojcik et al., "How allogenic factors affect succession in glacier forefields," *Earth-Sci. Rev.* **218**, 103642 (2021).
22. J. A. Robbins and J. A. Matthews, "Use of ecological indicator values to investigate successional change in boreal to high-alpine glacier-foreland chronosequences, southern Norway," *Holocene* **24**(11), 1453–1464 (2014).
23. A. Zimmer et al., "Timelag between glacial retreat and upward migration alters tropical alpine communities," *Perspect. Plant Ecol. Evol. Syst.* **30**, 89–102 (2018).
24. K. Prach and G. Rachlewicz, "Succession of vascular plants in front of retreating glaciers in central Spitsbergen," *Pol. Polar Res.* **33**(4), 319–328 (2012).
25. R. Walcker et al., "Contribution of meandering rivers to natural carbon fluxes: evidence from the Ucayali River, Peruvian Amazonia," *Sci. Total Environ.* **776**(1), 146056 (2021).
26. A. Fischer et al., "Vegetation dynamics in Alpine glacier forelands tackled from space," *Sci. Rep.* **9**(1), 1–13 (2019).
27. R. Hock and M. Huss, "Glaciers and climate change," Chapter 9 in *Climate Change*, 3rd ed., T. M. Letcher, Ed., pp. 157–176, Elsevier (2021).
28. A. Rabatel et al., "Changes in glacier equilibrium-line altitude in the western Alps from 1984 to 2010: evaluation by remote sensing and modeling of the morpho-topographic and climate controls," *Cryosphere* **7**(5), 1455–1471 (2013).
29. C. J. Tucker, "Red and photographic infrared linear combinations for monitoring vegetation," *Remote Sens. Environ.* **8**(2), 127–150 (1979).
30. Y. Sohn and R. M. McCoy, "Mapping desert shrub rangeland using spectral unmixing and modeling spectral mixtures with TM data," *Photogramm. Eng. Remote Sens.* **63**(6), 707–716 (1997).
31. E. Cossart et al., "Les variations glaciaires en Haute-Durance (Briançonnais, Hautes-Alpes) depuis la fin du XIXe siècle: mise au point d'après les documents d'archives et la lichénométrie," *Quaternaire* **17**, 75–92 (2006).
32. P. Lardeux et al., "Glaciological and geomorphological map of Glacier Noir and Glacier Blanc, French Alps," *J. Maps* **12**(3), 582–596 (2016).
33. E. Thibert, M. Bonnefoy-Demongeot, and F. Nouguier, "Cartographie des retraits glaciaires des Glacier Blanc et Glacier Noir depuis 1815 Application à l'établissement de chronoséquences de colonisation de la végétation," p. 23 (2019).
34. D. Turner, A. Lucieer, and C. Watson, "An automated technique for generating georectified mosaics from ultra-high resolution unmanned aerial vehicle (UAV) imagery, based on structure from motion (SfM) point clouds," *Remote Sens.* **4**, 1392–1410 (2012).

35. M. R. James et al., "Guidelines on the use of structure from motion photogrammetry in geomorphic research," *Earth Surf. Process. Landf.* **44**(10), 2081–2084 (2019).
36. I. Sola, M. González-Audícana, and J. Álvarez-Mozos, "Multi-criteria evaluation of topographic correction methods," *Remote Sens. Environ.* **184**, 247–262 (2016).
37. A. K. Saha et al., "Land cover classification using IRS LISS III Image and DEM in a rugged terrain: a case study in Himalayas," *Geocarto Int.* **20**(2), 33–40 (2005).
38. W. Liu and F. Yamazaki, "Object-based shadow extraction and correction of high-resolution optical satellite images," *IEEE J. Sel. Top. Appl. Earth Obs. Remote Sens.* **5**(4), 1296–1302 (2012).
39. O. Conrad et al., "System for automated geoscientific analyses (SAGA) v. 2.1.4," *Geosci. Model Dev.* **8**, 1991–2007 (2015).
40. D. W. Roberts and S. V. Cooper, "Concepts and techniques of vegetation mapping," in *Land Classif. Based Veg.: Appl. Resour. Manage.*, Ogden, Utah (1989).
41. L. Breiman, "Random forests," *Mach. Learn.* **45**, 5–32 (2001).
42. A. Liaw and M. Wiener, "Classification and regression by randomForest," *R News* **2**(3), 18–22 (2002).
43. B. M. Greenwell, "pdp: an R package for constructing partial dependence plots," *R J.* **9**(1), 421–436 (2017).
44. J. P. Ormsby, B. J. Choudhury, and M. Owe, "Vegetation spatial variability and its effect on vegetation indices," *Int. J. Remote Sens.* **8**(9), 1301–1306 (1987).
45. T. Phulpin, J. Noilhan, and M. Stoll, "Parameters estimates of a soil vegetation model using AVHRR data," in *Proc. 4th AVHRR Data Users Meeting*, Rothenburg, Germany, pp. 125–129, Darmstadt: EUMETSAT EUM P 06 (1990).
46. W. P. Kustas, C. S. T. Daughtry, and P. J. V. Oevelen, "Analytical treatment of the relationships between soil heat flux/net radiation ratio and vegetation indices," *Remote Sens. Environ.* **46**(3), 319–330 (1993).
47. K.-P. Wittich and O. Hansing, "Area-averaged vegetative cover fraction estimated from satellite data," *Int. J. Biometeorol.* **38**, 209–215 (1995).
48. G. Gutman and A. Ignatov, "The derivation of the green vegetation fraction from NOAA/AVHRR data for use in numerical weather prediction models," *Int. J. Remote Sens.* **19**(8), 1533–1543 (1998).
49. A. R. Huete, R. D. Jackson, and D. F. Post, "Spectral response of a plant canopy with different soil backgrounds," *Remote Sens. Environ.* **17**(1), 37–53 (1985).
50. J. R. Dymond et al., "Percentage vegetation cover of a degrading rangeland from SPOT," *Int. J. Remote Sen.* **13**(11), 1999–2007 (1992).
51. T. N. Carlson and D. A. Ripley, "On the relation between NDVI, fractional vegetation cover, and leaf area index," *Remote Sens. Environ.* **62**(3), 241–252 (1997).
52. Z. Jiang et al., "Analysis of NDVI and scaled difference vegetation index retrievals of vegetation fraction," *Remote Sens. Environ.* **101**(3), 366–378 (2006).
53. Z. Jiang and A. Huete, "Linearization of NDVI based on its relationship with vegetation fraction," *Photogramm. Eng. Remote Sens.* **76**(8), 965–975 (2010).
54. X. Chen et al., "Detecting post-fire burn severity and vegetation recovery using multitemporal remote sensing spectral indices and field-collected composite burn index data in a ponderosa pine forest," *Int. J. Remote Sens.* **32**(23), 7905–7927 (2011).
55. M. Verdonen et al., "Periglacial vegetation dynamics in arctic Russia: decadal analysis of tundra regeneration on landslides with time series satellite imagery," *Environ. Res. Lett.* **15**, 105020 (2020).
56. P. T. Fretwell et al., "Detecting and mapping vegetation distribution on the Antarctic Peninsula from remote sensing data," *Polar Biol.* **34**, 273–281 (2011).
57. M. E. Sotille et al., "Evaluation of UAV and satellite-derived NDVI to map maritime Antarctic vegetation," *Appl. Geogr.* **125**, 102322 (2020).
58. S. W. Todd and R. M. Hoffer, "Responses of spectral indices to variations in vegetation cover and soil background," *Photogramm. Eng. Remote Sens.* **64**(9), 915–921 (1998).
59. N. Rodriguez-Alvarez et al., "Soil moisture and vegetation height retrieval using GNSS-R techniques," in *IEEE Int. Geosci. Remote Sens. Symp.*, pp. III-869–III-872 (2009).

60. K. Edokossi et al., "GNSS-reflectometry and remote sensing of soil moisture: a review of measurement techniques, methods, and applications," *Remote Sens.* **12**(4), 614 (2020).
61. C. Haselwimmer and P. Fretwell, "Field reflectance spectroscopy of sparse vegetation cover on the Antarctic Peninsula," in *First Workshop Hyperspectral Image Signal Process. Evol. Remote Sens.*, pp. 1–4 (2009).
62. M. Calvino-Cancela and J. Martin-Herrero, "Spectral discrimination of vegetation classes in ice-free areas of Antarctica," *Remote Sens.* **8**(10), 856 (2016).
63. L. C. Bliss, "Vascular plant vegetation of the southern circumpolar region in relation to Antarctic, alpine, and arctic vegetation," *Can. J. Bot.* **57**(20), 2167–2178 (1979).
64. A. Marcinkowska-Ochtyra et al., "Subalpine and alpine vegetation classification based on hyperspectral APEX and simulated EnMAP images," *Int. J. Remote Sen.* **38**(7), 1839–1864 (2017).
65. J. A. Matthews, *The Ecology of Recently-Deglaciated Terrain: A Geological Approach to Glacier Forelands*, Cambridge University Press (1992).
66. J. Eichel, D. Draebing, and N. Meyer, "From active to stable: paraglacial transition of Alpine lateral moraine slopes," *Land Degrad. Dev.* **29**(11), 4158–4172 (2018).
67. H. A. Viles et al., "Biogeomorphological disturbance regimes: progress in linking ecological and geomorphological systems," *Earth Surf. Process. Landf.* **33**(9), 1419–1435 (2008).
68. D. Corenblit, J. Steiger, and J. Tabacchi, "Biogeomorphologic succession dynamics in a Mediterranean river system," *Ecography* **33**(6), 1136–1148 (2010).
69. L. Lindner and L. Marks, "Types of debris slope accumulations and rock glaciers in South Spitsbergen," *BOREAS* **14**(2), 139–153 (1985).
70. J. A. Bradley, J. S. Singarayer, and A. M. Anesio, "Microbial community dynamics in the forefield of glaciers," *Proc. R. Soc. B* **281**(1795), 20140882 (2014).
71. B. Elberling et al., "Distribution and dynamics of soil organic matter in a Antarctic dry valley," *Soil Biol. Biochem.* **38**(10), 3095–3106 (2006).
72. D. P. Roy et al., "A general method to normalize Landsat reflectance data to nadir BRDF adjusted reflectance," *Remote Sens. Environ.* **176**, 255–271 (2016).

Arthur Bayle is an ecologist and remote sensing engineer studying vegetation dynamics in cold regions. His studies contributed to improve the understanding of greening trends in alpine and arctic environment and how associated drivers are affecting these dynamics. He is currently working toward his PhD in the Grenoble-Alpes University, France.

Erwan Roussel is a geomorphologist studying climate change impacts on proglacial environments with a focus on geomorphic and vegetation responses of glacier forelands to glacial retreat.

Bradley Z. Carlson is an ecologist specialized in the use of remote sensing to study the dynamics of high mountain vegetation in response to climate changes in the Alps.

Dov Corenblit is a biogeomorphologist studying feedbacks between vegetation dynamics and Earth surface processes and landforms. His interdisciplinary studies contribute to the development of an eco-evolutionary perspective for establishing the functional linkages between geomorphology, ecology, and evolutionary biology.

Biographies of the other authors are not available.